IEEE Access
Multidisciplinary | Rapid Review | Open Access Journal

Received 25 February 2024, accepted 6 March 2024, date of publication 14 March 2024, date of current version 20 March 2024.

Digital Object Identifier 10.1109/ACCESS.2024.3375943

RESEARCH ARTICLE

Gearbox Fault Diagnosis Method Based on PSM-BN

YUAN SHANQIN, WANG JINHUA, AND CAO JIE
School of Electrical Engineering and Information Engineering, Lanzhou University of Technology, Lanzhou, Gansu 730050, China
Corresponding author: Yuan Shanqin (212085400007@lut.edu.cn)

This work was supported in part by the Fund Project: National Natural Science Foundation of China under Grant 62063020 and Grant 61763028, in part by the National Key Research and Development Plan Project under Grant 2020YFB1713600, and in part by the Natural Science Foundation of Gansu Province under Grant 20JR5RA463.

ABSTRACT The gearbox fault diagnosis method based on deep learning lacks good interpretability, and the complexity of the model leads to prolonged diagnostic times. Based on this, this paper proposes a Compute Unified Device Architecture (CUDA) parallelized Bayesian Network (BN) approach for gearbox fault diagnosis. To address the problem of the Max-Min Hill-Climbing (MMHC) algorithm easily getting trapped in local optima during BN learning, this paper introduces the Snake Optimization (SO) algorithm. This algorithm utilizes multiple individuals to represent potential solutions and updates their positions at each iteration, employing a diversity search strategy to avoid falling into local optima. In response to the high complexity and poor real-time inference of BN fault diagnosis methods, this paper utilizes the CUDA platform as a development framework and employs a CPU+GPU heterogeneous parallel BN to improve the operational efficiency of the model, thereby enhancing the real-time capability of fault diagnosis. Finally, validation is conducted on the gearbox dataset from Southeast University, demonstrating that the proposed method achieves a diagnosis accuracy of 99.7% on 800 fault samples with a training time of 10.4 seconds. Compared to traditional methods, this approach exhibits significant advantages in diagnostic accuracy and training speed, effectively enhancing the accuracy and stability of fault diagnosis.

INDEX TERMS Bayesian network, CUDA parallelism fault diagnosis, maximum-minimum hill climbing algorithm, snake optimization algorithm.

I. INTRODUCTION

Fault diagnosis plays a pivotal role in industrial production. However, with the increasing automation and complexity of modern industrial systems, traditional fault diagnosis methods based on mathematical models and expert knowledge have become inefficient and overly intricate. In the context of big data in industry, data-driven fault diagnosis methods leverage large-scale monitoring data and employ advanced machine learning techniques to achieve real-time monitoring and fault diagnosis of industrial equipment, thereby circumventing the need for complex mechanistic models and minimizing reliance on expert knowledge. To address potential faults in industrial equipment, a series of data-driven fault diagnosis methods have been proposed in relevant research. Among them, Zhang et al. [1] addressed the detection and diagnosis of various faults in battery packs, proposing a method based on curve Manhattan distance and voltage difference analysis. Zhang et al. [2] tackled the challenge of detecting early faults in analog circuits, presenting a method based on kernel entropy component analysis and one-against-one least squares support vector machines. Zhang et al. [3] tackled the difficulty of how to effectively localize faults in analog circuit diagnosis, proposing an improved wavelet transform feature extraction and multi-kernel extreme learning machine approach. Simultaneously, He et al. [4] dealt with extracting effective features from fault signals in analog circuits, proposing a method based on cross-wavelet transform and variational Bayesian matrix factorization. Those aforementioned methods have employed advanced signal processing and intelligent diagnostic techniques, enhancing the accuracy and reliability

The associate editor coordinating the review of this manuscript and approving it for publication was Guillermo Valencia-Palomo.

of fault diagnosis. However, challenges persist regarding the limited applicability of these methods, as well as the complexity and high computational costs of algorithms. Therefore, data-driven fault diagnosis methods have emerged as the mainstream in recent years, particularly for critical components such as gearboxes. Gearboxes, serving as crucial mechanical components in aerospace, automotive, and heavy industrial applications, endure substantial dynamic loads within mechanical transmission systems [5]. Their unexpected failures often result in significant maintenance costs and even catastrophic events [6]. Thus, accurately identifying potential fault distributions and further determining their health status are essential to ensure the proper operation of the entire mechanical transmission system.

In recent years, both domestic and international scholars have conducted extensive research on gearbox fault diagnosis [7], [8], which includes deep learning-based diagnostic methods such as Transfer Learning (TL), Generative Adversarial Networks (GAN), Graph Neural Networks (GNNs), Transformers, and others have been widely applied. These methods, particularly, exhibit significant advantages in scenarios with limited samples and the diagnosis of subtle potential faults. Addressing the issue of low diagnostic accuracy due to insufficient fault samples, Jamil et al. [9] proposed a deep-boosting transfer learning approach with the prevention of negative transfer. Zhao et al. [10] introduced a method combining joint distribution adaptation transfer learning and deep belief networks for the diagnosis of rotating machinery faults. Su et al. [11] presented an improved GAN-based approach for small-sample gearbox fault diagnosis. Yang et al. [12] proposed a GAN-based oversampling method to achieve gearbox fault diagnosis with a small dataset. While these methods have to some extent addressed the issue of limited samples in fault diagnosis, the interpretability of the diagnostic models remains a challenge. In addressing the challenge of detecting latent faults in fault diagnosis, Yu et al. [13] proposed a novel method employing a rapid deep graph convolutional network for diagnosing faults in wind turbine generators. Jiang et al. [14] introduced a bearing fault diagnosis approach based on a multi-head graph attention network. Tang et al. [15] presented an integrated visual Transformer model based on wavelet transform and soft voting method, enhancing the diagnostic accuracy and generalization capability for bearing faults. Ding et al. [16] proposed a novel time-frequency Transformer model for gearbox fault diagnosis. While these methods have to some extent improved the detection capability of diagnostic models for latent faults, they have also increased the complexity of the diagnostic models, consequently reducing diagnostic speed. However, due to the inherent opacity of deep learning models, characterized by their decision-making processes and internal details, they are often regarded as black-box models. Additionally, the design and training processes of these diagnostic models are relatively intricate, involving complex parameter tuning that demands more computational resources, thereby resulting in poor real-time diagnostic performance. Consequently, enhancing the interpretability and real-time capability of the models becomes a crucial challenge.

BN can effectively deal with uncertainty problems based on probabilistic information by learning to discover the probabilistic relationships between fault modes and fault features from fault data. Constructing the topological structure for fault diagnosis through causal relationships not only provides a clearer understanding of the diagnostic process and decision basis but also enhances the interpretability of diagnostic results, which is crucial for realizing effective fault diagnosis and decision support. Therefore, researchers have widely used BNs in the field of fault diagnosis [17]. However, learning the optimal structure of BNs is challenging, and choosing an inappropriate structure may lead to inaccurate diagnostic results. Additionally, the inference and probability calculations of BN demand substantial computational resources, resulting in higher computational complexity and slower inference speeds. To address the problem that BN structure learning does not capture the probabilistic dependencies between observations well, Zhang et al. [18] proposed to use a binary encoding to represent the structure of a BN and apply a water-cycle algorithm to search for the structure. Chen and Hao [19] introduced a new method for learning the structure of BNs using a discrete firefly optimization algorithm. Veni and Kumar [20] presented an approach combining Bayesian optimization and integrated learning techniques by automatically tuning the hyperparameters of the classifier to maximize the accuracy and performance of bearing fault diagnosis in induction motors. Aiming at the time-consuming problem of conditional independence testing in the learning process of Bayesian structures, Quan et al. [21] introduced to use the MMHC algorithm to construct a BN to analyze the network relationship between COPD and its influencing factors. Jiang et al. [22] proposed a method based on minimum Bayesian risk reclassification and adaptive weighting, which obtains more accurate and reliable fault diagnosis results. Tao et al. [23] proposed a new parallelization method for conditional independence testing, where parallel algorithms can process multiple data points or sub-tasks at the same time, thus improving computational efficiency. The above method optimizes the BN structure to some extent, which improves diagnostic efficiency. These methods optimize the BN structure to some extent, enhancing diagnostic efficiency. Among them, the MMHC algorithm belongs to a hybrid BN learning approach, exhibiting stronger generalization compared to other methods. However, there are faces several challenges, including the tendency for the established models to fall into local optima and the typically high computational complexity associated with constructing Bayesian fault diagnosis networks, thereby impacting both the training speed and real-time diagnostic performance of the models.

Based on the above analysis, addressing the issue of BN structure learning prone to local optima, this paper proposes

utilizing the SO algorithm for a global search strategy to optimize the MMHC algorithm in constructing BN. Meanwhile, to tackle the problem of the high complexity in constructing BN leading to slow diagnostic speed, an approach involving heterogeneous parallelism is introduced to enhance the real-time capability of fault diagnosis. By distributing the process of searching for the optimal BN across different computing units for parallel execution, the search results are transmitted via the bus to the CPU, allowing for iterative refinement to obtain the optimal fault diagnosis model. While ensuring diagnostic accuracy, this approach effectively enhances the timeliness of training fault models, achieving a highly compatible relationship between diagnostic accuracy and modelling speed.

II. BN

Gearbox fault diagnosis usually involves uncertainties in the causes of faults, and BNs can effectively model these uncertainties, making the diagnosis more accurate and reliable, while BNs [24] graphically represent the dependencies between variables, and therefore have a high degree of interpretability.

A BN is composed of a directed acyclic graph G and a conditional probability distribution P. The graph $G = (V, E)$ encodes a set of independent relationships among variables $V = \{X_1, X_2, \cdots, X_n\}$ through the d-separation criterion and E represents the set of directed relationships among these variables. The joint probability distribution over the variable domain is factorized using the conditional probability distribution $\{p\,(X_i|pa_G(X_i))\}\, i \in \{1, 2, \cdots, n\}$ according to: $P(V) = P(X_1, X_2, \cdots X_n) = \prod_{i=1}^{n} p(X_i|pa_G(X_i))$.

The structural learning of BN is a crucial step in the entire modelling process, and the common BN structure learning methods are mainly divided into two categories: constraint-based methods and score-based search methods. Constraint-based methods offer more precise variable relationships, but their premise is that appropriate knowledge of the domain is required. Score-based search methods learn by searching for the optimal scoring structure among possible structures; however, their efficiency tends to be relatively low when dealing with a large structure space. Therefore, to overcome the limitations of the above methods, this paper adopts a hybrid algorithm, the MMHC algorithm [25] to construct the BN, which uses both domain knowledge to initialize the candidate structures and statistical scoring methods to select the final network structure, which overcomes the limitations of a single method and improves the accuracy of structure learning.

III. MMHC

The MMHC algorithm integrates dependency analysis and score-based search methods, consisting of two phases. In the first phase, the Max-Min Parent-Child (MMPC) algorithm is employed to determine the candidate parent-child node sets for each node, constructing an undirected framework for the BN structure. In the second stage, this paper employs a greedy hill-climbing algorithm to search and evaluate the obtained network structures, identifying the network structure with the highest score.

The MMPC algorithm employs a maximal-minimal heuristic strategy to identify the set of Candidate Parents and Children (CPC) [26] for the target variable T from a given dataset, which is divided into two stages. In the first stage, a correlation function is defined to ascertain the conditional dependency relationships between other variables and the target variable T under the given conditions of the CPC. The max-min heuristic selects the variable with the largest and smallest correlation with the target variable T into the CPC under the given CPC conditions. The first stage stops when all variables in the CPC except the variable are conditionally independent of the target variable T under the given CPC conditions. In the second stage, the variables in the CPC of the set of candidate parent-child nodes are tested and the wrong variables are excluded. For variable X in the CPC, if a subset S of the CPC exists, such as $Assoc(X, T|S)$, then the variable X is removed from the CPC.

The correlation function between variable X and variable T for a given set of variables T is defined as equation (1).

$$Assoc(X, T|Z) = 2 \sum_{a,b,c} N_{ijk}^{abc} ln \frac{N_{ijk}^{abc} N_k^c}{N_{ik}^{ac} N_{jk}^{bc}} \tag{1}$$

where N_{ijk}^{abc} is the number of samples in the dataset D that satisfy $X = aT = h$, and $Z = c$. The corresponding minimum correlation function is defined as equation (2).

$$MinAssoc(X, T, |Z) = \frac{min}{S \subseteq Z} Assoc(X, T|S) \tag{2}$$

where S is a subset of the variable set Z.

MMHC is a local search algorithm, however, in the case of a large structure space, the algorithm may fall into local optima due to the selection of different initial structures and the adoption of various search strategies. Therefore, when using MMHC for structural search, this method cannot guarantee the discovery of the globally optimal network structure.

IV. SO ALGORITHM

In this paper, the SO algorithm [27] is used to solve the problem that MMHC constructs a Bayesian fault diagnostic network which tends to fall into the local optimum. SO algorithm is a global search heuristic algorithm that explores the search space by simulating the behaviours of snakes to improve the diversity, searching ability and convergence. Snake search is divided into two phases: exploration and exploitation. In the exploration stage, when the environmental temperature is low and food is scarce, the snake conducts a global search for food. During the exploitation stage, when food is available and the temperature is high, the snake focuses on the local search to consume food. If food is available and the temperature is low, mating takes place. This contributes to the optimization of the MMHC algorithm,

preventing it from getting stuck in local optima and increasing the likelihood of achieving a global optimum.

A. MATHEMATICAL MODEL OF SO ALGORITHM

In the exploration phase, assuming an insufficient availability of food, the snake randomly moves towards the direction of food search, and the amount of food Q is counted by $0.5exp\left(\frac{t-T}{T}\right)$. T is the maximum number of iterations. Male and female exploratory behaviours are modelled as shown in equation (3) and equation (4):

$$X_{i,m}^{t+1} = X_{rand,m}^{t} \pm C_2 \times A_m \times ((X_{max} - X_{min}) \times rand + X_{min}) \tag{3}$$

$$X_{i,f}^{t+1} = X_{rand,f}^{t} \pm C_2 \times A_f \times ((X_{max} - X_{min}) \times rand + X_{min}) \tag{4}$$

where $X_{i,m}^{t+1}$, $X_{i,f}^{t+1}$ and denote the i th male and female, respectively. $X_{rand,m}^{t}$ and $X_{rand,f}^{t}$ are randomly selected positions of males and females from the overall population. t is the current iteration, $rand$ is a random value, and C_2 is a constant set to 0.05. A_m and A_f measure the ability of males and females to access food, calculated by $exp\left(\frac{-f_{rand,m}}{f_{i,m}}\right)$ $exp\left(\frac{-f_{rand,f}}{f_{i,f}}\right)$ and, respectively; $f_{rand,m}$ and $f_{rand,f}$ are the fitness values of $X_{rand,m}^{t}$ and $X_{rand,f}^{t}$, respectively, while $f_{i,m}f_{i,f}$ and are the fitness values of males and females, respectively.

During the development phase, it is assumed that food is available, and the next position is defined based on the environmental temperature ($TEMP$). The ambient temperature is defined by $exp\left(\frac{-t}{T}\right)$, and if the temperature is higher than a threshold, a new position for the male and female is localized using equation (5), which X_{food}^{t} represents the optimal individual position equal to 2.

$$X_{i,f,m}^{t+1} = X_{food}^{t} \pm C_3 \times TEMP \times rand \times (X_{food} - X_{i,f,m}^{t}) \tag{5}$$

Otherwise, the snake is in either combat or mating mode and switches randomly between these two modes, calculating the new position using equation (6) and equation (7) for combat mode and equation (8) and equation (9) for mating mode.

$$X_{i,m}^{t+1} = X_{i,m}^{t} \pm C_3 \times FM \times rand \times (X_{best,f} - X_{i,m}^{t}) \tag{6}$$

$$X_{i,f}^{t+1} = X_{i,f}^{t+1} \pm C_3 \times FF \times rand \times (X_{best,m} - X_{i,f}^{t+1}) \tag{7}$$

$$X_{i,m}^{t+1} = X_{i,m}^{t} \pm C_3 \times M_m \times rand \times (Q \times X_{i,f}^{t} - X_{i,m}^{t}) \tag{8}$$

$$X_{i,f}^{t+1} = X_{i,f}^{t} \pm C_3 \times M_f \times rand \times (Q \times X_{i,m}^{t} - X_{i,f}^{t}) \tag{9}$$

where FM and FF represent the combat abilities of males and females, calculated respectively by $exp\left(\frac{-f_{best,f}}{f_i}\right)$ and $exp\left(\frac{-f_{best,m}}{f_i}\right)$. M_m and M_f denote the mating abilities in male-female conflicts, also computed based on $exp\left(\frac{-f_{i,f}}{f_{i,m}}\right)$ and $exp\left(\frac{-f_{i,m}}{f_{i,f}}\right)$.

B. SO-MMHC

The SO algorithm guides the MMHC to construct a Bayesian fault diagnosis network by simulating the movement of the snake in the search space, which aims to prevent the Bayesian fault diagnosis network from falling into a local optimum when searching the solution space. The global optimization performance of constructing a Bayesian fault diagnosis network is enhanced by the global search property of the SO algorithm, and the specific algorithm steps are shown below.

Step 1: Randomly generate the locations of the initial snake population, with each snake representing a potential solution. $X_i^{(0)} \sim U(S)$ obeys a uniform distribution, where $X_i^{(0)}$ denotes the initial position of the ith snake and U denotes a uniform distribution;

Step 2: Initialize the BN structure using the MMHC algorithm, which includes 22 fault features of 5 fault types from the gearbox dataset of Southeast University $G = MMHC\_Initialize(Nodes, Edges)$;

Step 3: Define the search space including all legitimate BNs $S = \{G|G\ is\ effective\ BN\}$;

Step 4: Attain the global optimum by simulating the snake's exploration and exploitation stages in the search space. $X_i^{(t+1)} = X_i^{(t)} + \alpha \cdot Mov(X_i^{(t)}, X_{best}^{(t)})$, α is a step control parameter, $Mov(X_i^{(t)}, X_{best}^{(t)})$ is a function that simulates the snake's movement in the search space, and $X_{best}^{(t)}$ is the location of the global optimal solution;

Step 5: Update the current network structure, $G^{(t+1)} = US(G^{(t)}, X_i^{(t+1)})US$ are the functions for updating the network structure according to the position and movement direction of the snake;

Step 6: Calculate the model likelihood and penalty term score, denoted as

$$Score(G^{(t+1)}) = Likelihood(G^{(t+1)}) + Penalty(G^{(t+1)});$$

Step 7: Selecting the highest-scoring one as the next network architecture, denoted as $G^* = argmax_{G^{(t+1)}} Score(G^{(t+1)})$;

Step 8: Check if the stopping condition is satisfied, the stopping condition is reaching the maximum number of iterations or the highest score;

Step 9: Updating the global optimal solution so that the performance of different snakes can be compared, denoted as $X_{best}^{(t+1)} = argmax_i\ Score(G_i^{(t+1)})$;

Step 10: Repeating steps 3 to 9, repeating the steps of snake motion simulation, network structure updating, model evaluation and global optimal solution updating, until the stopping condition is satisfied. In each iteration, accumulate the structure scores, and at the end, divide by the number of runs to obtain the network structure with the highest average score;

Step 11: Output the constructed Bayesian fault diagnosis network structure G.

The above method combines the SO algorithm with the MMHC algorithm, focusing on the search and optimization phases of the BN structure, Specifically, in the initialization

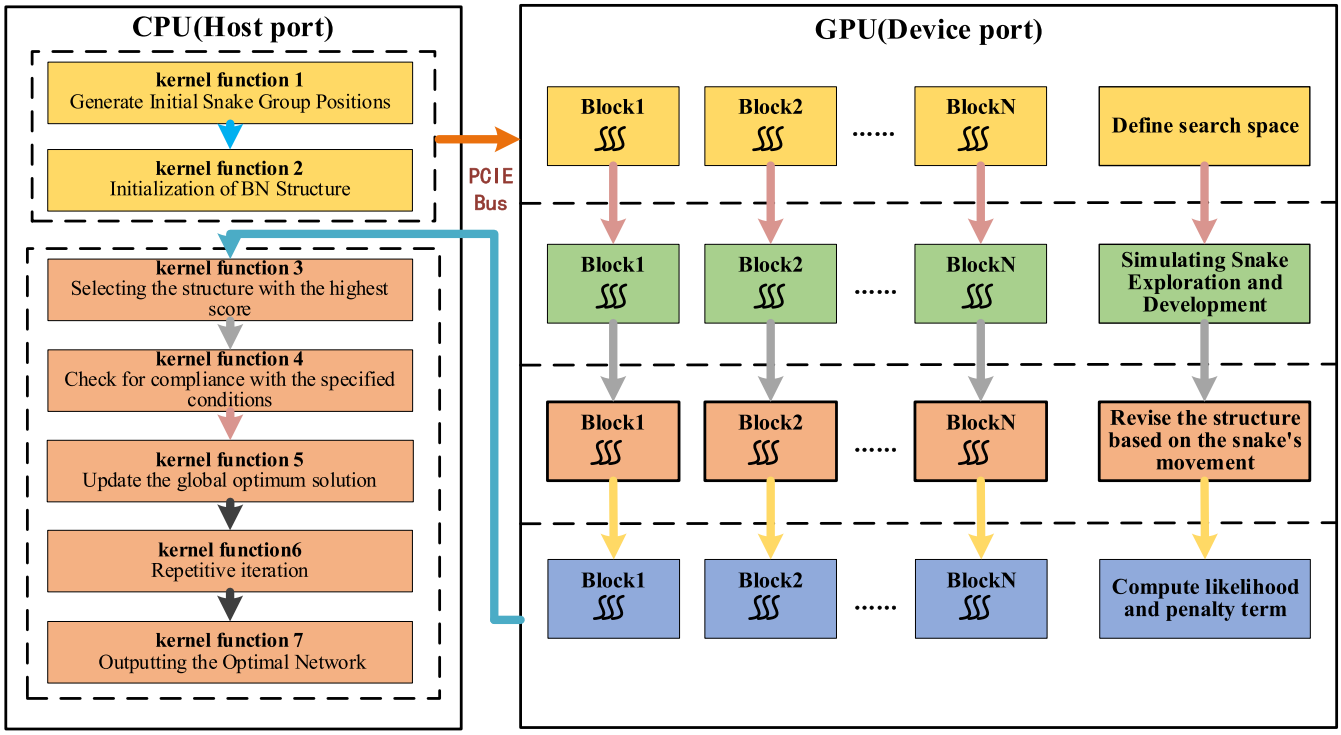

FIGURE 1. CPU-GPU heterogeneous parallel process.

and iterative optimization of the MMHC algorithm, which improves and guides the search process by simulating the snake's search strategy. It solves the problem that the MMHC algorithm is easy to falls into the local optimal solution when constructing the BN fault diagnosis model, but the method requires a large amount of computational resources, and the high computational cost makes this method unsuitable for fault diagnosis research with high real-time requirements. To solve this problem, this paper adopts a heterogeneous parallel method [28] based on CUDA to accelerate the diagnosis process.

V. CONSTRUCTING A BN FAULT DIAGNOSIS MODEL FOR SO-MMHC WITH HETEROGENEOUS PARALLELISM (PSM-BN)

To improve the real-time fault diagnosis, this paper adopts a heterogeneous parallel algorithm and utilizes the CUDA architecture to perform parallel computation on the GPU side. In the design of parallel algorithms, balancing the division granularity of computational tasks and the amount of computing, if the granularity is too small, the computational volume of a single task is small, which may lead to excessive waste of computational resources on the control and deployment of threads; if the granularity is too large, the computational volume of a single task is large, which may make the computational process of the parallelization is not high, wasting the resources of the threads. Therefore, in this paper, taking the computational capacity of GPU cores and the characteristics of the network construction process into account, the partition idea is adopted to recursively divide the computational tasks. The parallel process of the model is shown in Figure 1, the construction process is shown in Figure 2, and the specific algorithm steps are as follows.

Step 1: On the CPU side, the initial positions of the snake population are generated. The initial snake population positions can be represented as a matrix, where each row represents the initial position of a snake, and each column represents a value of network structure parameters. These initial positions can be randomly generated from a uniform distribution, denoted as $X_i^{(0)} \sim U(S)$, where $U(S)$ represents a uniform distribution;

Step 2: On the CPU side, the BN structure is initialized using the MMHC algorithm. This includes defining the search space and initializing the network structure parameters. The network encompasses five fault types and twenty-two fault features from the Southeast University gearbox dataset. Initialization is performed using the function

$$G = MMHC\_Initialize(Nodes, Edges);$$

Step 3: The initial positions of the snake population and the network structure are transferred to the GPU side. This includes transmitting the initial snake population positions and network structure generated in Steps 1 and 2 to the GPU, denoted as $Transfer\_to\_GPU(X_i^{(0)}, G)$;

Step 4: On the GPU side, the search space is defined, which encompasses all possibly valid BN structures. Each row in this space represents a network structure, with each column

representing a value of network structure parameters. This space is denoted as $S = \{G|G \text{ is a valid } BN\}$

Step 5: On the GPU side, the exploration and exploitation phases of snake movement within the search space are simulated. This is achieved by defining appropriate search space and movement functions. The movement function governs the direction and step size of the snake's movement within the search space, denoted as

$$X_i^{(t+1)} = X_i^{(t)} + \alpha \cdot Mov(X_i^{(t)}, X_{best}^{(t)}) Transfer\_to\_GPU(X_i^{(t+1)}$$

where α is the step size control parameter, and $Mov(X_i^{(t)}, X_{best}^{(t)})$ is the function governing the simulated snake's movement in the search space, and $X_{best}^{(t)}$ represents the global optimal solution position;

Step 6: On the GPU side, the concurrent update of current network structure parameters is performed based on the snake's movement within the search space. This can be achieved by defining appropriate GPU functions, denoted as $G^{(t+1)} = US\ \text{GPU}(G^{(t)}, X_i^{(t+1)}) Transfer\_to\_CPU(G^{(t+1)})$ where the *US* GPU is a GPU function responsible for updating the network structure based on the snake's position and movement direction;

Step 7: On the GPU side, parallel computation of the model likelihood and penalty scores for each network structure is performed, and the results are transferred to the CPU side for selecting the optimal structure, denoted as

$Fitness\_on\_GPU(G^{(t+1)}) = Likelihood\_on\_GPU(G^{(t+1)})$ and $Transfer\_to\_CPU(Fitness\_on\_GPU)$;

Step 8: On the CPU side, the score information transmitted from the GPU is received, and the structure with the highest score is selected as the next step's network structure, denoted as $G^* = argmax_{G^{(t+1)}} Fitness\_on\_CPU(G^{(t+1)})$;

Step 9: On the CPU side, check for the satisfaction of stopping conditions, whether the maximum iteration count is reached, or the highest score is achieved;

Step 10: On the CPU side, the global optimum solution is updated. If the score of the current network structure is higher than the previous global optimum solution, the CPU updates the global optimum solution, denoted as

$$X_{best}^{(t+1)} = argmax_i Fitness\_on\_CPU(G_i^{(t+1)});$$

Step 11: Repeat steps from 3 to 9, iteratively perform snake motion simulation, network structure updates, model evaluation, and global optimum solution updates until the termination conditions are met. In each iteration, accumulate the structure scores, and at the end, divide by the number of runs to obtain the network structure with the highest average score;

Step 12: The finalized Bayesian fault diagnosis network structure G is outputted. This network structure is determined based on the global optimum solution obtained during the optimization process.

These steps integrate the SO algorithm, MMHC algorithm, and CUDA parallel computing to accelerate the SO algorithm for improving the computational efficiency of the MMHC algorithm, especially when searching for the structure of large-scale BNs, to avoid falling into local optimal solutions. To reduce the data transmission delay, this paper uses a polling algorithm for workflow management and scheduling on GPUs so that computation and data copying can be performed simultaneously. In the asynchronous execution, the device execution and storage operation work simultaneously, which improves the overall operation efficiency of the algorithm and mitigates the impact of data transmission on the computational efficiency of the GPU. The detailed steps of optimizing the MMHC-based BN construction using the CUDA parallel SO algorithm are described below:

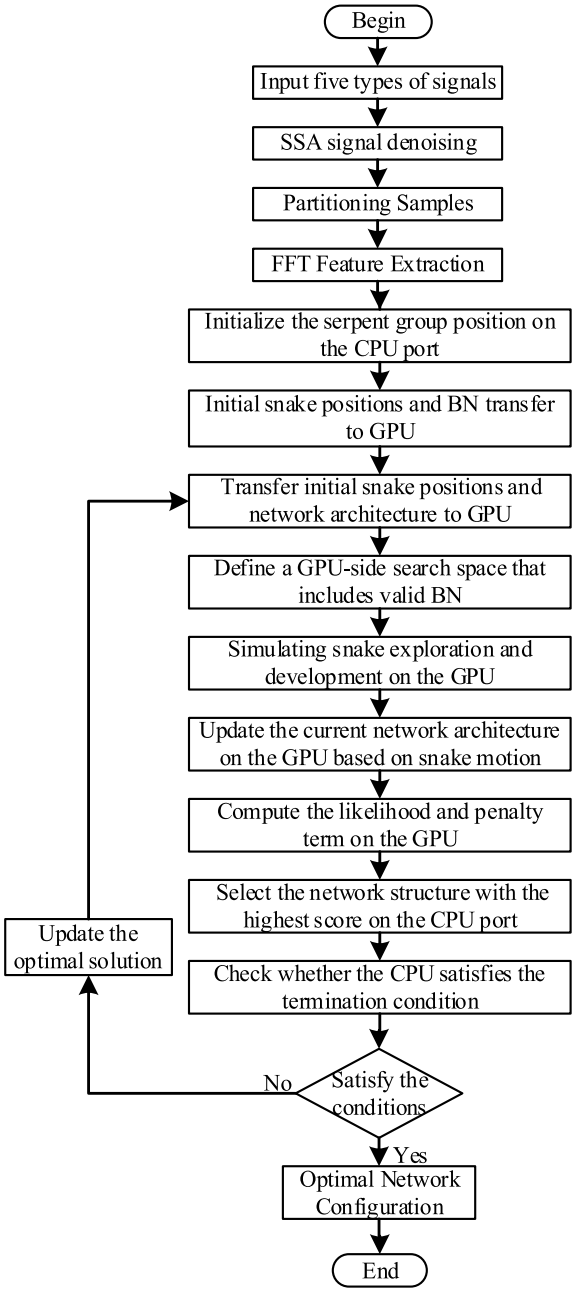

FIGURE 2. Overall flowchart of the algorithm.

By combining the SO algorithm and the MMHC algorithm with CUDA parallel computing, the space of BN structures can be searched more quickly to optimize the gearbox troubleshooting problem, while reducing the risk of locally optimal solutions and improving computational efficiency. The algorithm is effective in managing the performance complementarity between CPU and GPUs, improving the portability of the algorithm by collecting the required information for scheduling decisions through a message-passing system.

VI. EXPERIMENTAL RESULTS AND ANALYSIS

To validate the diagnostic performance of the method proposed in this paper, the experimental data this paper uses a set of gearbox vibration data provided by Southeast University, which contains the fault vibration signals recorded during the operation of the gearbox. The method proposed in this paper is validated and illustrated by the following experiments to demonstrate the reliability and accuracy of the proposed method under different data sets.

A. EXPERIMENTAL DATA

The dataset used in this experiment is the gearbox dataset publicly available from Southeast University, which was collected through a dynamic simulation system [29] of a transmission chain, as depicted in Figure 3. The experimental setup primarily consists of a motor, motor controller, planetary gearbox, parallel-axis gearbox, and brake. Seven vibration sensors of model 608A11 are utilized to collect vibration data along the x, y, and z axes of the planetary and parallel-axis gearboxes, as well as along the z-axis of the motor. The sampling frequency is 5120 Hz, with data collection performed under two operating conditions: 20 Hz (1200 rpm) with a load setting of 0 V (0 Nm), and 30 Hz (1800 rpm) with a load setting of 2 V (7.32 Nm).

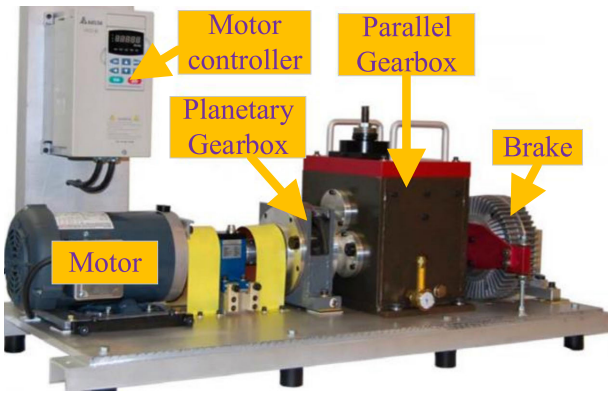

FIGURE 3. Data acquisition device for gearbox fault dataset.

In this study, experiments were conducted using a subset of data collected under the second operating condition of 30 Hz-2 V. The fault types considered include inner race crack (IF), outer race crack (OF), healthy gear (N), gear foot crack (GF1), and gear root crack (GF2). During the data processing stage, 22 time-domain and frequency-domain features were extracted for each sample, including mean, standard deviation, slope, energy, and spectral peak frequency etc, to fully exploit the information within the data and enhance the diagnostic performance of the fault models. The same diagnostic model is experimented under four groups of different sample sizes, with sample sizes of 200, 400, and 800 for a single type in each group of experiments, and 1000 sample points for each sample. A total of five classifications, which include four fault types and one normal condition, with total sample sizes of 1000, 2000, and 4000 for each set of experiments to validate the diagnostic performance of different diagnostic models under different sample sizes, and each classification is randomly divided into training and test samples according to a ratio of 3:1, which is used to validate the accuracy of the proposed fault diagnostic model.

B. EX ANALYSIS OF EXPERIMENTAL RESULTS MENTAL

To validate the effect of Singular Spectrum Analysis (SSA), this paper adds Gaussian white noise to the test set of the current signal as shown in equation (10).

$$y(t) = x(t) + n(t) \tag{10}$$

where $y(t)$ represents the signal after adding the noise, and $x(t)$ represents the original signal, $n(t)$ and represents Gaussian white noise with mean 0 and variance σ^2. The formula for SNR equation is shown as equation (11).

$$SNR_{dB} = 10\log_{10}\left(\frac{P_{\text{signal}}}{P_{\text{noise}}}\right) \tag{11}$$

where "P_{signal}" and "P_{noise}" refer to the power values of the signal and noise, respectively. The results after the introduction of noise are illustrated in Figure 4.

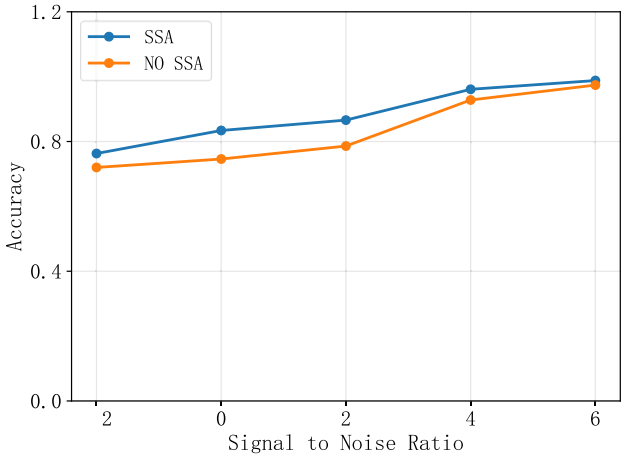

FIGURE 4. Diagnostic accuracy under SSA and NO SSA with different signal-to-noise ratios.

As can be seen from Figure 4, at all Signal to Noise Ratio (SNR) levels, the SSA [30] method used in this paper has superior diagnostic performance than the method without SSA. The experimental results show that for both methods,

the performance increases as the SNR increases. However, the performance of the method in this paper is more stable when the noise increases, and at all SNR levels, the method used in this paper shows a significant performance improvement relative to not using SSA, which suggests that SSA is effective in dealing with noise and improving diagnostic performance. This is because SSA is effective in separating the trend and periodic components of the signal, thus reducing the effect of noise. The experimental results demonstrate that SSA improves the diagnostic performance of the model in a noisy environment.

To assess the performance of the proposed method, in this paper, classification experiments are carried out by classifying the dataset when the sample size of each class is 400, experimental validation is carried out on the test set, and the results include precision(P), recall(R), and F1-score($F1$). The precision is calculated as shown in equation (12).

$$P = \frac{n_{\mathrm{TP}}}{n_{\mathrm{TP}} + n_{\mathrm{FP}}} \tag{12}$$

The recall rate is expressed by the equation (13) as indicated.

$$R = \frac{n_{\mathrm{TP}}}{n_{\mathrm{TP}} + n_{\mathrm{FN}}} \tag{13}$$

The fraction is expressed as per the f equation (14).

$$F1 = \frac{2P \times R}{P + R} = \frac{2n_{\mathrm{TP}}}{2n_{\mathrm{TP}} + n_{\mathrm{FP}} + n_{\mathrm{FN}}} \tag{14}$$

where n_{TP} is the number of true cases, and n_{FP} is the number of false positive cases, and n_{FN} is the number of false negative cases. The results of the evaluation are shown in Table 1.

TABLE 1. Evaluation of PSM-BN on the gearbox dataset.

Dataset	Evaluation Metrics	IF	OF	N	GF1	GF2
Gearbox Dataset	Precision	0.99	1.0	1.0	1.0	1.0
	recall ratio	0.99	1.0	1.0	1.0	1.0
	F1	0.995	1.0	1.0	1.0	1.0

In the gearbox dataset, the accuracy and recall rates for all classes exceed 99%, even reaching 100%. This indicates that the classifier accurately identifies each class without any instances of misclassification or false negatives. The majority of classes achieve an F1 score of 1, demonstrating a well-balanced trade-off between precision and recall. This implies that the classifier maintains high accuracy and recall simultaneously, delivering excellent performance across all class categorizations. However, the F1 score for the IF class is slightly lower than that of other classes, indicating some misclassification by the classifier within the IF category, leading to a slight imbalance between precision and recall. In summary, the experimental results demonstrate that the proposed method exhibits excellent diagnostic performance and reliability in fault diagnosis tasks within industrial production. The diagnostic precision and recall for GF1, GF2, and N have all achieved very high levels.

To evaluate the performance of this classifier, a confusion matrix is used in this paper for analysis. The diagnostic model is shown in Figure 5, and the corresponding results of the confusion matrix are shown in Figure 6.

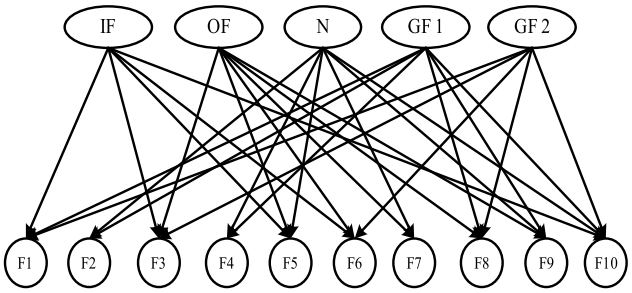

FIGURE 5. BN model of gearbox fault diagnosis.

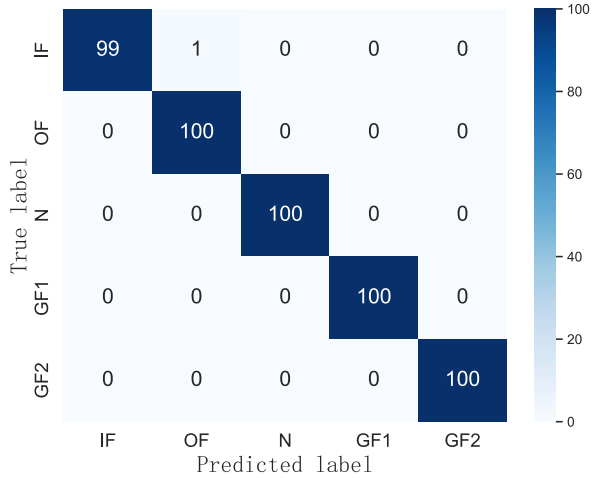

FIGURE 6. Confusion matrix of gearbox fault diagnosis.

In Figure 5, BN's F1-F10 represent features including mean, rectified mean, variance, standard deviation, root mean square, waveform factor, peak factor, pulse factor, root amplitude, and crest factor, respectively. From the confusion matrix, it can be observed that the diagonal elements are 99, 100, 100, 100, and 100, indicating high classification accuracy across the five fault types. Only one sample each from the gearbox IF and OF classes exhibits confusion in classification, while the rest of the samples are correctly classified. This suggests that the model achieves high accuracy in predicting each fault type, demonstrating excellent classification performance for these five fault types.

To comprehensively evaluate the seven different algorithms, this study conducted tests on 200, 400, and 800 samples, recording their diagnostic accuracy and model training time. Comparative experiments primarily contrasted PSM-BN with PM-BN (without SO), Transfer Learning-based Convolutional Neural Networks (TCNN),

African Vultures Optimization Algorithm combined with Stochastic Configuration Networks (AVOA-SCN), Deep Transfer Learning (Deep-TL), Kurtosis Weighting Fusion and Parallel Lightweight Convolutional Networks (KW-PLCN), and Information Fusion and Parallel Lightweight Convolutional Networks (IF-PLCN). These comparisons aimed to showcase their advantages in multi-fault diagnosis under varying sample sizes. The experimental results are presented in Table 2.

TABLE 2. Comparative experiments of the gearbox dataset with 200, 400, and 800 samples.

Comparative Experiments	accuracy	time	accuracy	time	accuracy	time
PSM-BN	97.21%	4.8s	99.79%	5.1s	99.74%	10.4s
PM-BN(NO)	95.33%	4.6s	96.77%	4.9s	97.58%	10.1s
AVOA-SCN[31]	95.19%	9.2s	97.32%	10.2s	98.58%	15.9s
TCNN[32]	90.14%	8.9s	95.42%	9.9s	98.64%	14.8s
DEEP-TL[29]	93.91%	7.3s	95.73%	9.1s	96.40%	13.2s
KW-PLCN[33]	95.93%	8.3s	95.99%	9.3s	96.94%	14.5s
IF-PLCN[33]	95.99%	8.4s	97.44%	8.8s	98.23%	13.9s

Table 2 presents the diagnostic accuracy and training time of different classification algorithms across varying sample sizes. It is evident that as the sample size increases, the diagnostic accuracy of most methods improves. Notably, PSM-BN consistently maintains the highest diagnostic accuracy across different sample sizes, indicating superior diagnostic performance compared to other methods. This suggests that the proposed method outperforms others due to its simpler model architecture, as it does not utilize a so algorithm. While PM-BN exhibits slightly better diagnostic time compared to PSM-BN, there is a significant gap in diagnostic accuracy. Therefore, it can be inferred that the proposed method effectively improves diagnostic accuracy. However, it is worth mentioning that TCNN and Deep-TL exhibit relatively lower accuracy when the sample size is small. Nevertheless, as the sample size increases, their accuracy gradually improves. AVOA-SCN and IF-PLCN demonstrate higher accuracy under large sample sizes, albeit requiring relatively longer training times. Overall, PSM-BN demonstrates faster training speeds across different sample sizes and achieves the highest accuracy, further confirming the excellent performance of the PSM-BN algorithm in diagnostic tasks.

To assess the stability of the different models, this paper conducts 20 independent experiments on each model, each time using a different training set. In this paper, the average accuracy of these experiments was calculated on the test set and summarized in Table 3. Table 3 demonstrates the average accuracy, t-statistics, and p-values for each model.

From the table above, it can be observed that PSM-BN, utilizing the SO algorithm, demonstrates superior performance in the experiments. PSM-BN exhibits higher average

TABLE 3. Multiple experiment accuracy results.

Experimental Methods	Precision	t-statistic	p-value
PSM-BN	96.94±1.66	/	/
PM-BN	94.50+1.71	1.68	0.045
TCNN	94.60±1.75	1.57	0.361
AVOA-SCN	91.12±1.13	14.17	0.044
Deep-TL	92.19±1.90	13.84	0.036
KW-PLCN	93.10±2.43	1.82	0.434
IF-PLCN	94.10±1.43	1.22	0.473

precision compared to PM-BN. Through t-test analysis, the p-value is calculated as 0.043, which is less than the significance level of 0.05, indicating a statistically significant difference. This suggests that the SO algorithm optimizes the model to better adapt to specific tasks, thereby enhancing performance. Therefore, it can be concluded that the proposed method has high diagnostic performance. Additionally, PSM-BN shows higher average precision compared to TCNN. In terms of the t-statistic, there is no significant difference in precision between the two methods (t-statistic=1.53), with a p-value of 0.351, exceeding the typical significance level of 0.05. This suggests that the difference is likely due to random factors, lacking sufficient evidence to reject the null hypothesis of no significant difference in precision between the two methods. Compared to AVOA-SCN, PSM-BN demonstrates superior precision. In terms of the t-statistic, the difference in precision between the two methods is not significant (t-statistic=2.17), with a p-value of 0.344, higher than the usual significance level of 0.05. This lack of evidence leads to the inability to reject the null hypothesis of no significant difference in precision between the two methods. Additionally, PSM-BN exhibits superior precision than Deep-TL. In terms of the t-statistic, there is a significant difference in precision between the two methods (t-statistic=13.82), with a p-value of 0.036, lower than the typical significance level of 0.05, further confirming the rejection of the null hypothesis of no significant difference in precision between the two methods. However, compared to IF-PLCN, PSM-BN does not exhibit a significant difference in precision. Both the t-statistic and p-value fail to provide sufficient evidence to support or reject the hypothesis of a significant difference in precision between the two methods. In summary, PSM-BN demonstrates a significant advantage in precision compared to other methods, indicating optimal performance. Therefore, the proposed PSM-BN method exhibits higher precision in the experiments and possesses significant performance advantages.

VII. CONCLUSION

This paper proposes a Fault Diagnosis Method based on PSM-BN to address the issues of insufficient interpretability and long diagnostic time in deep learning diagnostic methods.

This method not only possesses strong interpretability but also effectively reduces the training time of the algorithm by combining precise inference algorithms for probabilistic graphical models with GPU parallelization techniques, thus improving the diagnostic efficiency of existing fault diagnosis methods. Regarding the construction of BN models, this paper presents a solution to the problem of the MMHC algorithm easily falling into local optima. By employing the SO algorithm, where each individual represents a potential solution and their positions are updated at each iteration to maintain multiple individuals, the dilemma of falling into local optima is effectively avoided, thereby enhancing the diagnostic quality of the BN. Another crucial issue is how to balance diagnostic complexity and real-time performance in Bayesian fault diagnosis methods. Considering that traditional serial computing cannot meet real-time requirements, this paper adopts the CUDA platform as the development framework and utilizes the divide-and-conquer approach to implement a CPU+GPU heterogeneous parallel BN fault diagnosis method, thereby improving the real-time performance of fault diagnosis. Ultimately, through experiments on multiple fault datasets, it is demonstrated that the proposed method exhibits significant advantages over traditional methods in terms of diagnostic accuracy and modelling speed with the same number of fault samples.

REFERENCES

[1] C. Zhang, S. Zhao, Z. Yang, and Y. He, "A multi-fault diagnosis method for lithium-ion battery pack using curvilinear Manhattan distance evaluation and voltage difference analysis," *J. Energy Storage*, vol. 67, Sep. 2023, Art. no. 107575, doi: 10.1016/j.est.2023.107575.

[2] C. L. Zhang, Y. G. He, L. Zuo, J. P. Wang, and W. He, "A novel approach to diagnosis of analog circuit incipient faults based on KECA and OAO LSSVM," *Metrol. Meas. Syst.*, vol. 22, no. 2, pp. 251–262, Jun. 2015, doi: 10.1515/mms-2015-0025.

[3] C. Zhang, Y. He, T. Yang, B. Zhang, and J. Wu, "An analog circuit fault diagnosis approach based on improved wavelet transform and MKELM," *Circuits, Syst., Signal Process.*, vol. 41, no. 3, pp. 1255–1286, Mar. 2022, doi: 10.1007/s00034-021-01842-2.

[4] W. He, Y. He, B. Li, and C. Zhang, "Feature extraction of analogue circuit fault signals via cross-wavelet transform and variational Bayesian matrix factorisation," *IET Sci., Meas. Technol.*, vol. 13, no. 2, pp. 318–327, Mar. 2019, doi: 10.1049/iet-smt.2018.5432.

[5] F. Leaman, C. M. Vicuña, and E. Clausen, "A review of gear fault diagnosis of planetary gearboxes using acoustic emissions," *Acoust. Aust.*, vol. 49, no. 2, pp. 265–272, Jun. 2021, doi: 10.1007/s40857-021-00217-6.

[6] T. Wang, Q. Han, F. Chu, and Z. Feng, "Vibration based condition monitoring and fault diagnosis of wind turbine planetary gearbox: A review," *Mech. Syst. Signal Process.*, vol. 126, pp. 662–685, Jul. 2019, doi: 10.1016/j.ymssp.2019.02.051.

[7] D. Liu, L. Cui, and W. Cheng, "Fault diagnosis of wind turbines under nonstationary conditions based on a novel tacho-less generalized demodulation," *Renew. Energy*, vol. 206, pp. 645–657, Apr. 2023, doi: 10.1016/j.renene.2023.01.056.

[8] G. F. Wang and F. Wang, "Research on fault diagnosis of wind power planetary gearbox based on optimized EFD algorithm," *J. Tianjin Univ.*, vol. 56, no. 4, pp. 355–360, 2023.

[9] F. Jamil, T. Verstraeten, A. Nowé, C. Peeters, and J. Helsen, "A deep boosted transfer learning method for wind turbine gearbox fault detection," *Renew. Energy*, vol. 197, pp. 331–341, Sep. 2022, doi: 10.1016/j.renene.2022.07.117.

[10] H. Zhao, X. Yang, B. Chen, H. Chen, and W. Deng, "Bearing fault diagnosis using transfer learning and optimized deep belief network," *Meas. Sci. Technol.*, vol. 33, no. 6, Jun. 2022, Art. no. 065009, doi: 10.1088/1361-6501/ac543a.

[11] Y. Su, L. Meng, X. Kong, T. Xu, X. Lan, and Y. Li, "Small sample fault diagnosis method for wind turbine gearbox based on optimized generative adversarial networks," *Eng. Failure Anal.*, vol. 140, Oct. 2022, Art. no. 106573, doi: 10.1016/j.engfailanal.2022.106573.

[12] S. Yang, Y. Zhou, X. Chen, C. Deng, and C. Li, "Fault diagnosis of wind turbines with generative adversarial network-based oversampling method," *Meas. Sci. Technol.*, vol. 34, no. 4, Apr. 2023, Art. no. 044004, doi: 10.1088/1361-6501/acad20.

[13] X. Yu, B. Tang, and K. Zhang, "Fault diagnosis of wind turbine gearbox using a novel method of fast deep graph convolutional networks," *IEEE Trans. Instrum. Meas.*, vol. 70, pp. 1–14, 2021, doi: 10.1109/TIM.2020.3048799.

[14] L. Jiang, X. Li, L. Wu, and Y. Li, "Bearing fault diagnosis method based on a multi-head graph attention network," *Meas. Sci. Technol.*, vol. 33, no. 7, Jul. 2022, Art. no. 075012, doi: 10.1088/1361-6501/ac56f1.

[15] X. Tang, Z. Xu, and Z. Wang, "A novel fault diagnosis method of rolling bearing based on integrated vision transformer model," *Sensors*, vol. 22, no. 10, p. 3878, May 2022, doi: 10.3390/s22103878.

[16] Y. Ding, M. Jia, Q. Miao, and Y. Cao, "A novel time–frequency transformer based on self–attention mechanism and its application in fault diagnosis of rolling bearings," *Mech. Syst. Signal Process.*, vol. 168, Apr. 2022, Art. no. 108616, doi: 10.1016/j.ymssp.2021.108616.

[17] F. Xu, Z. Pan, and R. Xia, "E-commerce product review sentiment classification based on a naïve Bayes continuous learning framework," *Inf. Process. Manage.*, vol. 57, no. 5, Sep. 2020, Art. no. 102221, doi: 10.1016/j.ipm.2020.102221.

[18] C. Zhang, Z. Liu, and L. Zhang, "Wind turbine blade bearing fault detection with Bayesian and adaptive Kalman augmented Lagrangian algorithm," *Renew. Energy*, vol. 199, pp. 1016–1023, Nov. 2022, doi: 10.1016/j.renene.2022.09.030.

[19] J. G. Chen and G. W. Hao, "Research on the fault diagnosis of wind turbine gearbox based on Bayesian networks," in *Practical Applications of Intelligent Systems* (Advances in Intelligent and Soft Computing), vol. 124, Shanghai, China. Berlin, Germany: Springer, 2011, pp. 217–223.

[20] K. S. K. Veni and N. S. Kumar, "Diagnosis of bearing fault in induction motor using Bayesian optimization-based ensemble classifier," *Electr. Eng.*, vol. 2023, pp. 1–11, Oct. 2023.

[21] D. Quan, J. Ren, H. Ren, L. Linghu, X. Wang, M. Li, Y. Qiao, Z. Ren, and L. Qiu, "Exploring influencing factors of chronic obstructive pulmonary disease based on elastic net and Bayesian network," *Sci. Rep.*, vol. 12, no. 1, May 2022, Art. no. 7563, doi: 10.1038/s41598-022-11125-8.

[22] R. Jiang, J. Yu, and V. Makis, "Optimal Bayesian estimation and control scheme for gear shaft fault detection," *Comput. Ind. Eng.*, vol. 63, no. 4, pp. 754–762, Dec. 2012, doi: 10.1016/j.cie.2012.04.015.

[23] L. Tao, L. Sun, Y. Wu, C. Lu, J. Ma, Y. Cheng, and M. Suo, "Multi-signal fusion diagnosis of gearbox based on minimum Bayesian risk reclassification and adaptive weighting," *Measurement*, vol. 187, Jan. 2022, Art. no. 110358, doi: 10.1016/j.measurement.2021.110358.

[24] H. Habibi, I. Howard, and R. Habibi, "Bayesian fault probability estimation: Application in wind turbine drivetrain sensor fault detection," *Asian J. Control*, vol. 22, no. 2, pp. 624–647, Mar. 2020, doi: 10.1002/asjc.1973.

[25] W. Song, H. Gong, Q. Wang, L. Zhang, L. Qiu, X. Hu, H. Han, Y. Li, R. Li, and Y. Li, "Using Bayesian networks with max-min hill-climbing algorithm to detect factors related to multimorbidity," *Frontiers Cardiovascular Med.*, vol. 9, Aug. 2022, Art. no. 984883, doi: 10.3389/fcvm.2022.984883.

[26] L. Lara Carrion and K. A. Bramstedt, "Exploring the ethical complexity of pediatric organ transplant candidates and COVID-19 vaccination: Tensions between autonomy and beneficence, children and parents," *Pediatric Transplantation*, vol. 27, no. 1, Feb. 2023, Art. no. e14408, doi: 10.1111/petr.14408.

[27] L. Cui and J. Liao, "Intelligent power grid energy supply forecasting and economic operation management using the snake optimizer algorithm with bigur-attention model," *Frontiers Energy Res.*, vol. 11, Sep. 2023, Art. no. 1273947, doi: 10.3389/fenrg.2023.1273947.

[28] F. Zheng, H. Tan, and F. Tian, "Parallel performance analysis for CUDA-based co-rank framework on bipartite graphs heterogeneous network," in *Proc. 17th Int. Symp. Distrib. Comput. Appl. Bus. Eng. Sci. (DCABES)*, Oct. 2018, pp. 12–15, doi: 10.1109/DCABES.2018.00014.

[29] S. Shao, S. McAleer, R. Yan, and P. Baldi, "Highly accurate machine fault diagnosis using deep transfer learning," *IEEE Trans. Ind. Informat.*, vol. 15, no. 4, pp. 2446–2455, Apr. 2019, doi: 10.1109/TII.2018.2864759.

[30] X. Wang and B. W. Ling, "Length reduction of singular spectrum analysis with guarantee exact perfect reconstruction via block sliding approach," *IEEE Access*, vol. 8, pp. 170311–170321, 2020, doi: 10.1109/ACCESS.2020.3023468.
[31] R. J. H. Y. F. Fan and Q. S. Yang, "Gearbox fault diagnosis based on VMD and AVOA-SCN," *Manuf. Technol. Mach. Tools*, vol. 10, no. 12, pp. 19–25, 2023.
[32] Y. Huiyu and Z. Chao, "Gear fault diagnosis method based on transformer and convolutional neural network," *J. Mech. Electr. Eng.*, early access, pp. 1–11, 2024. [Online]. Available: https://link.cnki.net/urlid/33.1088.TH.20231024.1734.008
[33] Y. Guan, Z. Meng, D. Sun, J. Liu, and F. Fan, "Rolling bearing fault diagnosis based on information fusion and parallel lightweight convolutional network," *J. Manuf. Syst.*, vol. 65, pp. 811–821, Oct. 2022, doi: 10.1016/j.jmsy.2022.11.012.

YUAN SHANQIN was born in Shaanxi, China. He received the B.E. degree in measurement and control technology and instrumentation from Xi'an Aeronautical University, Xi'an, China, in 2019. He is currently pursuing the M.S. degree in electronic and information engineering with Lanzhou University of Technology, Lanzhou, China. His research interests include intelligent algorithm analysis and modeling, and fault diagnosis based on machine learning.

WANG JINHUA was born in Gansu, China. She received the B.S. degree from Xi'an University of Science and Technology, Xi'an, China, in 2001, the M.S. degree from Lanzhou University of Technology, Lanzhou, China, in 2010, and the Ph.D. degree in pattern recognition and intelligent systems.

Since June 2001, she has been engaged in teaching and scientific research with the Department of Electronic Information Engineering, School of Telecommunications, Lanzhou University of Technology. Her research interests include intelligent information processing, deep learning algorithm research and application, multi-source information fusion, and intelligent fault diagnosis. She is a member of the Information Fusion Sub-Committee of the Chinese Society of Aeronautics and Astronautics and the China Computer Society. She is a Communication Review Expert with the National Natural Science Foundation of China.

CAO JIE was born in Gansu, China. She received the B.Tech. degree from Gansu Institute of Technology, Lanzhou, China, in 1987, and the M.Tech. degree from Xi'an Jiaotong University, in 1994.

Since March 1996, she has been the Deputy Director of the Technical Basic Course Department, the Electrical Engineering Department, and the Personnel Department; and the Deputy Dean, the Dean, and the Director of the Academic Affairs Office of the School. She is currently a Professor, a Ph.D. Tutor, a second-level Professor, a Ph.D. Supervisor, and the Vice President of Lanzhou University of Technology. Her research interests include information fusion and pattern recognition.